Inorganic Chemistry

Article

pubs.acs.org/IC

Site-Isolated Redox Reactivity in a Trinuclear Iron Complex

Emily V. Eames and Theodore A. Betley*

Department of Chemistry and Chemical Biology, Harvard University, 12 Oxford Street, Cambridge, Massachusetts 02138, United States

Supporting Information

ABSTRACT: The symmetric, high-spin triiron complex (^{Ph}L)-Fe_3(THF)$_3$ reacts with mild chemical oxidants (e.g., Ph_3C-X, I_2) to afford an asymmetric core, where one iron bears the halide ligand (^{Ph}L)Fe_3X(L) and the hexadentate (^{Ph}L = MeC(CH_2NPh-*o*-NPh)$_3$) ligand has undergone significant rearrangement. In the absence of a suitable trapping ligand, the chlorine and bromine complexes form (μ-X)$_2$-bridged structures of the type [(^{Ph}L)Fe_3(μ-X)]$_2$. In the trinuclear complexes, the halide-bearing iron site sits in approximate trigonal-bipyramidal (tbp) geometry, formed by two (^{Ph}L) anilides and an exogenous solvent molecule. The two distal iron atoms reside in distorted square-planar sites featuring a short Fe−Fe separation at 2.301 Å, whereas the distance to the tbp site is substantially elongated (2.6−2.7 Å). Zero-field, ^{57}Fe Mössbauer analysis reveals the diiron unit as the locus of oxidation, while the tbp site bearing the halide ligand remains divalent. Magnetic data acquired for the series reveal that the oxidized diiron unit comprises a strongly coupled $S = {}^3/_2$ unit that is weakly ferromagnetically coupled to the high-spin ($S = 2$) ferrous site, giving an overall $S = {}^7/_2$ ground state for the trinuclear units.

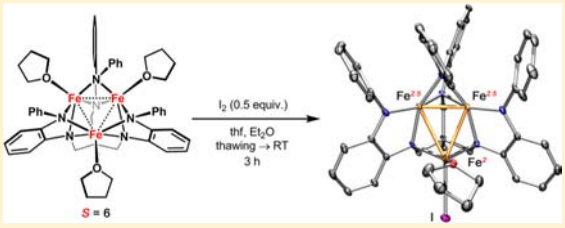

I. INTRODUCTION

While the collective function of polynuclear, metalloenzyme cofactors is well-described,[1] the functions of each individual metal site within the cofactor are difficult to ascertain. Undoubtedly, neighboring metals influence that cofactor reactivity by altering substrate coordination modes and buttressing redox changes and charge distribution within the cofactor.[1a,2] We[3] and others[4] are pursuing a class of coordination complexes that feature polynuclear cores to elucidate how transition metals can cooperatively mediate redox processes and to establish what types of reactivities are possible with multiple redox reservoirs available. Utilizing a simple, hexadentate amine-based platform, we have observed facile construction of polynuclear complexes. Transamination reactions of divalent metal precursors with the amine ligand afford trinuclear metal complexes with a broad range of molecular spin states ($S = 1-6$), which vary as a function of the ligand architecture.[3a,b,g] In the iron-based complexes, the use of the sterically unencumbered proton-capped ligand (^{H}L)$^{6-}$ gave rise to core-delocalized redox activity,[3a] whereas the use of the silylamide ligand (^{tbs}L)$^{6-}$ gave rise to atom-transfer reactivity to the triiron core, maintaining an open-shell electronic configuration.[3b] Herein we present redox reactivity of the maximally high-spin ($S = 6$) triiron complex[3g] (^{Ph}L)Fe_3(THF)$_3$ [**1**; ^{Ph}L = MeC(CH_2NPh-*o*-NPh)$_3$] that gives rise to asymmetric oxidation products where coordination change occurs at an isolated ferrous site and a distal diiron unit undergoes redox changes.

II. EXPERIMENTAL SECTION

Physical Measurements. All of the measurements for the metal complexes were made under anaerobic conditions. Elemental analyses were performed by Complete Analysis Laboratories, Inc., Parsippany, NJ, or Robertson Microlit Laboratories, Madison, NJ. ^{1}H and ^{13}C NMR spectra were recorded on a Varian Unity/Inova 500B or a Varian Mercury 400B NMR spectrometer with chemical shifts (δ ppm) referenced to a residual NMR solvent. UV−vis spectra were recorded on a Varian Cary 50 UV−vis spectrometer using quartz cuvettes. Near-IR spectra were recorded on a PerkinElmer Lambda 750 high-performance UV−vis spectrometer.

Magnetic measurements were recorded using a Quantum Design MPMS-5S, MPMS-XL, or MPMS SQUID VSM magnetometer. Samples were prepared by placing the powdered sample in Lilly no. 4 gel capsules and soaking thoroughly with melted eicosane wax to ensure complete immobilization of the sample particulates. The capsules were suspended in the magnetometer in plastic straws. All manipulations were performed under an atmosphere of dinitrogen. Direct-current (dc) magnetic susceptibility data were collected in the temperature range 2−300 K under fields of 0.1, 0.5, 1, and 2 T. Magnetization data were acquired at 1.8−10 K under fields of 1, 2, 3, 4, 5, 6, and 7 T. Susceptibility data were corrected for the diamagnetic contribution of a blank sample consisting of the bag or wax, capsule, and straw at the correct field and temperature, as well as the constitutive corrections from Pascal's constants. The molar magnetic susceptibility (χ_m) was calculated by converting the magnetization (M) obtained from the magnetometer to a molar susceptibility using the multiplication factor [molecular weight (MW)]/[sample weight (m) × field strength (H)]. All samples were measured at least twice. All samples were checked for ferromagnetic impurities by collecting a field dependence curve at 100 K, and samples were rejected if any deviation from linearity was observed.

^{57}Fe Mössbauer spectra were measured on a constant-acceleration spectrometer (SEE Co., Minneapolis, MN) with a Janis SVT-100 cryostat. Isomer shifts are quoted relative to α-iron foil (<25 μm thick)

Received: June 11, 2012
Published: September 18, 2012

at room temperature. Samples were prepared using approximately 30 mg of sample suspended in paratone-N oil. The temperatures were controlled using a LakeShore 321 autotuning temperature controller. Data were collected at 95 K and analyzed using an in-house package written by E. R. King in *Igor Pro* (Wavemetrics). While it is not possible to definitively and precisely determine the isomer shift and quadrupole splittings in the presence of nearly identical overlapping peaks, the data for each compound were modeled based on the arbitrary assumption that the doublet with greater isomer shift has smaller quadrupole splitting. This assumption yields a simulation in which the isomer shifts, rather than the quadrupole splittings, are most nearly equal, a choice that seems justified in light of the fact that, in many of the spectra observed, the lowest-velocity peaks appear coalesced into a single site.

Preparation of [(^{Ph}L)Fe$_3$Cl]$_2$ (2). **1** (300 mg, 301 μmol) was dissolved in tetrahydrofuran (THF; 100 mL) and frozen in the glovebox cold well. Triphenylmethyl chloride (88.5 mg, 1.05 equiv) was added in 10 mL of THF to the thawing solution, and the resulting black solution was immediately placed under vacuum, with stirring, to remove volatiles. The dried product was dissolved in benzene and filtered rapidly to remove a pale, insoluble byproduct. The product is only briefly soluble in benzene, apparently because the initial product is benzene-soluble (^{Ph}L)Fe$_3$Cl(THF); as THF dissociates, the sparingly soluble chloride-bridged complex **2** precipitates from solution. To ensure a good yield, the solvent was removed, and benzene was added a second time to facilitate further precipitation of product in the absence of dissociated THF. The product was collected on a fritted glass funnel and washed with copious benzene and diethyl ether to remove the quinoid dimer Ph$_3$C(C$_6$H$_5$)CPh$_2$. It is usually possible to collect a second batch of product by drying the washes under vacuum and again precipitating from benzene. The yield from the first two collections was 125 mg (50%). NMR is not reported for the dimer because only the monomeric form is soluble. X-ray-quality crystals were grown from a concentrated, filtered benzene solution of the initial soluble product at room temperature. Anal. Calcd for C$_{41}$H$_{36}$Fe$_3$N$_6$Cl: C, 60.37; H, 4.45; N, 10.30. Found: C, 60.29; H, 4.34; N, 10.21.

Preparation of (^{Ph}L)Fe$_3$Cl(py) (3). A thawing solution of 1% (w/w) pyridine (py) in benzene (1.1 g, 140 μmol, 1.4 equiv) was added to solid **2** (100 mg, 100 μmol, 1 equiv) and stirred for 2 h. The resulting solution was filtered to remove a small amount of pale insoluble material, and volatiles were removed under vacuum. The resulting black powder was collected on a fritted glass funnel, washed with diethyl ether, and dried under vacuum. Yield: 90 mg (84%). X-ray-quality crystals were grown from a concentrated filtered solution in benzene at room temperature. ^{1}H NMR (C$_6$D$_6$, 500 MHz, δ, ppm): 160, 52, 31, 30, 26, 19, 11, 9, 4.5, −1, −3.5, −27, −77, −89, −92, −153. Anal. Calcd for C$_{46}$H$_{41}$Fe$_3$N$_7$Cl: C, 61.74; H, 4.62; N, 10.96. Found: C, 62.06; H, 4.58; N, 10.82.

Preparation of [(^{Ph}L)Fe$_3$Br]$_2$ (4). **1** (300 mg, 301 μmol) was dissolved in THF (100 mL) and frozen in the glovebox cold well. Triphenylmethyl bromide (97 mg, 1 equiv) was added in 10 mL of THF to the thawing solution, and the resulting black solution was immediately placed under vacuum, with stirring, to remove volatiles. The dried material was dissolved in benzene and filtered rapidly to remove a pale, insoluble byproduct. The dissolved species is only briefly soluble in benzene because the bromine-bridged complex **4** precipitates from solution. To ensure a good yield, the solvent was removed, and benzene was added a second time to facilitate further precipitation of the product in the absence of dissociated THF. The product was collected on a fritted glass funnel and washed with copious benzene and diethyl ether to remove the quinoid dimer Ph$_3$C(C$_6$H$_5$)CPh$_2$. A second batch of product was obtained by drying the washes under vacuum and again precipitating from benzene. The yield from the first two collections was 150 mg (58%). X-ray-quality crystals were grown from a concentrated, filtered benzene solution of the initial soluble product at room temperature. NMR is not reported for **4** because only the solvated form is soluble. Anal. Calcd for C$_{41}$H$_{36}$Fe$_3$N$_6$Br: C, 57.25; H, 4.22; N, 9.77. Found: C, 57.14; H, 4.15; N, 9.72.

Preparation of (^{Ph}L)Fe$_3$Br(THF) (5). Solid **4** (100 mg, 58 μmol, 1 equiv) was dissolved in THF (10 mL) at −35 °C, and the solution was filtered to remove any insoluble material. The resulting solution was concentrated to saturation (~3 mL), and diethyl ether (~7 mL) was added. The solution was stored at −35 °C to promote crystallization. The product was collected on a fritted glass funnel, washed with diethyl ether, and then dried under vacuum. Yield: 85 mg (78%). X-ray-quality crystals were grown from a concentrated solution in THF at −35 °C. ^{1}H NMR (C$_6$D$_6$, 500 MHz, δ, ppm): 104, 58, 43, 40, 32, 30, 20, 17, 13, 11, 9.5, 2, 0, −7, −28, −40, −72, −88, −95, −113, −149, −246. Anal. Calcd for C$_{45}$H$_{44}$Fe$_3$N$_6$OBr: C, 57.97; H, 4.76; N, 9.01. Found: C, 57.82; H, 4.94; N, 8.87.

Preparation of (^{Ph}L)Fe$_3$I(THF) (6). **1** (90 mg, 90.3 μmol) was dissolved in THF (25 mL) and frozen in the glovebox cold well. Iodine (11.4 mg, 1 equiv) was added in 5 mL of THF to the thawing solution, and the resulting black solution was immediately placed under vacuum, with stirring, until the solution had concentrated to a volume of ~2 mL. The resulting solution was filtered to remove a small amount of pale insoluble material, and additional THF (~2 mL) was added to fully dissolve the product. The solution was again concentrated to 2 mL and stored at −35 °C for 4 h. The solution was decanted, and the crystalline black product was washed twice with cold THF and dried under vacuum. Yield: 50 mg (88%). X-ray-quality crystals were grown from a concentrated filtered solution in benzene at room temperature. ^{1}H NMR (C$_6$D$_6$, 500 MHz, δ, ppm): 104, 35, 32, 28, 21, 11.6, 10.1, 8.9, −31, −75, −85, −89, −166. Anal. Calcd for C$_{45}$H$_{44}$Fe$_3$N$_6$IO: C, 55.19; H, 4.53; N, 8.58. Found: C, 54.89; H, 4.46; N, 8.54.

III. RESULTS AND DISCUSSION

Chemical oxidation of **1** can be readily effected by the treatment with 1 equiv of triphenylmethyl chloride (Ph$_3$CCl) in THF, producing 0.5 equiv of the quinoid dimer Ph$_3$C(C$_6$H$_5$)-CPh$_2$ (identified by ^{1}H NMR; Scheme 1).[5] The oxidized

Scheme 1

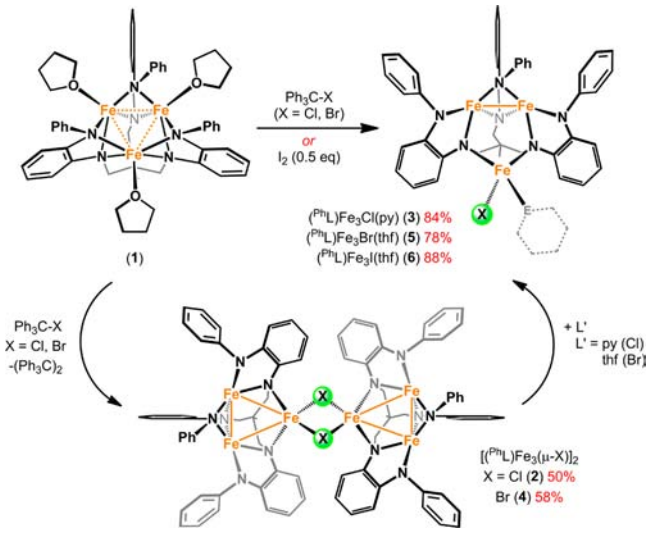

trinuclear complex was precipitated from benzene, affording the chloride-bridged product **2** or the trinuclear product **3**, following treatment with py (Scheme 1). Oxidation of **1** with triphenylmethyl bromide likewise produced both the halide-bridged products **4** and solvated trinuclear **5** from THF or benzene solutions, whereas the reaction of **1** with 0.5 equiv of iodine in THF exclusively gave the trinuclear product **6**. Single crystals for X-ray diffraction analysis were obtained by allowing a solution of each compound in benzene to stand at room

dx.doi.org/10.1021/ic301241s | *Inorg. Chem.* 2012, 51, 10274−10278

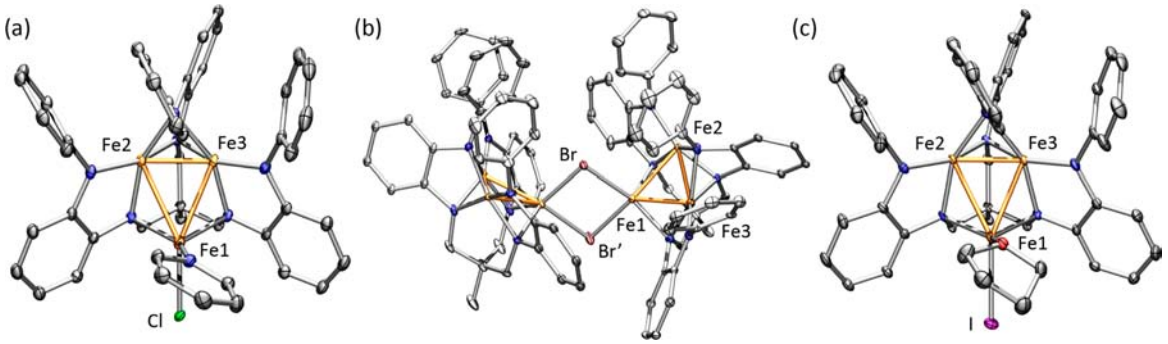

Figure 1. Solid-state structures for (a) **3**, (b) **4**, and (c) **6** with the thermal ellipsoids set at the 50% probability level (hydrogen atoms and solvent molecules are omitted for clarity) Color code: Fe, orange; C, black; N, blue; O, red; Cl, green; Br, brown; I, magenta. Bond lengths (Å) for **3**: Fe1−Fe2 2.7303(8), Fe1−Fe3 2.6534(8), Fe2−Fe3 2.2955(8), Fe1−Cl 2.3333(11), Fe1−N_{py} 2.066(3). Bond lengths (Å) for **4**: Fe1−Fe2 2.5871(7), Fe1−Fe3 2.5873(7), Fe2−Fe3 2.3504(7), Fe1−Br1 2.5715(6), Fe1−Br2 2.4670(6), Fe1−Fe1 3.5810(11). Bond lengths (Å) for **6**: Fe1−Fe2 2.6026(10), Fe1−Fe3 2.6971(11), Fe2−Fe3 2.3079(10), Fe1−I 2.6695(9), Fe1−O 2.024(4).

temperature (**2**, **3**, and **5**) or by cooling (−35 °C) a THF solution (**4** and **6**).

The chemical compositions of the oxidized complexes **2**−**6** were confirmed by single-crystal X-ray diffraction analysis. Representative examples of the solid-state structures for these species are provided in Figure 1. For the trinuclear complexes **3**, **5**, and **6**, the molecular structure reveals three salient features: (1) two molecules of THF are lost from **1**, (2) the hexaanilido (^{Ph}L) ligand has substantially altered its binding mode, and (3) the halide ligand from chemical oxidation is bound to a single iron site. The halide-bearing iron (Fe1 in Figure 1a) is nearly trigonal-bipyramidal (accounting for M−M interactions), where two ligand anilides and py form the trigonal plane and the chlorine atom caps the pyramid, positioned trans to the diiron portion of the trinuclear core. The remaining two iron atoms (Fe2 and Fe3) are each bound to four ligand anilide units, forming an intermediate geometry between the tetrahedral and square-planar locally at each iron, with a close Fe−Fe contact [Fe2−Fe3 2.2955(8) Å] in the axial site. The two remaining M−M contacts [Fe1−Fe2 2.7303(8) Å; Fe1−Fe3 2.6534(8) Å] are substantially elongated compared with the average metal separation in **1** [2.491(1) Å].[3g] The trinuclear core asymmetry is maintained in the trinuclear bromide and iodide structures [see Figure S4 in the Supporting Information (SI) and Figure 1c, respectively]. The bond metrics within the (^{Ph}L) ligand *o*-phenylenediamide units are consistent with those in the closed-shell dianion state (see Tables S3−S7 in the SI).[6]

The two hexanuclear products **2** and **4** exhibit the same structural distortions evident in the trinuclear complexes **3**, **5**, and **6**. One iron binds the halide ligands, while the ^{Ph}L ligand distorts to engender nearly square-planar binding modes to the two remaining iron sites. The short Fe2−Fe3 contact is maintained in both of the bridged hexanuclear complexes [2.3410(5) Å in **2** and 2.3504(7) Å in **4**]. While the Fe2−Fe3 separation is modestly elongated from the trinuclear species, the average Fe1−Fe2 and Fe1−Fe3 separations are substantially shorter [average (Å): 2.5849(5), **2**; 2.5872(7), **4**] than the distances observed in **3**, **5**, and **6**. The halide-bearing iron (Fe1 in **4** shown in Figure 1b) is more tetrahedral than the same site in the trinuclear complexes. The dihedral angle between Br−Fe1−Br and Fe2−Fe1−Fe3 is 67.85° (68.18° in **2**), creating a twist between the two trinuclear subunits.

The one-electron oxidation of **1** results in a [$Fe^{II}_2Fe^{III}$] formulation; however, the locus of oxidation (the halide-bearing iron, diiron unit, or ligand residue) was not immediately apparent. A representative zero-field ^{57}Fe Mössbauer spectrum obtained at 90 K for complex **3** is presented in Figure 2a. The spectrum reveals three distinct quadrupole doublets of equal intensity [δ, $|\Delta E_Q|$ (mm s^{-1}): 0.83, 1.67, 33%; 0.29, 2.44, 33%; 0.20, 2.79, 33%]. The isomer shift of the first component is consistent with a ferrous assignment and is comparable to the isomer shift found in **1** [δ, $|\Delta E_Q|$ (mm s^{-1}): 0.79, 1.25].[3g] The two remaining quadrupole doublets are considerably shifted from **1** and feature considerably larger quadrupole-splitting parameters. The significantly lowered isomer shift indicates an increase in the formal oxidation state, suggesting that oxidation occurs within the diiron unit. The similarity between the isomer shifts for the two iron atoms in the diiron unit indicates that the one-electron oxidation is substantially delocalized, yielding a mixed-valent diiron unit (i.e., $[Fe_2]^{5+}$). Thus, while Fe1 may bear the halide in **3**, the distal diiron unit (Fe2−Fe3) is the locus of oxidation, giving the formal oxidation assignment as $[Fe^{2+}(Fe_2)^{5+}]$. The spectrum for **3** is highly representative of the entire series **2**−**6** (see Figures S7−S11 in the SI), indicating that this oxidation distribution is maintained throughout the series.

The solution magnetic moments obtained for the soluble trinuclear complexes (e.g., μ_{eff} = 7.94 μ_B for **3**, 295 K, C_6D_6) indicate that the oxidized products maintain an open-shell configuration, although reduced from a maximally high-spin state ($S = {}^{13}/_2$), which would exhibit a spin-only moment of 13.96 μ_B. To probe the magnetic behavior of complexes **2**−**6** further, variable-temperature dc susceptibility data were collected in the temperature range of 5−300 K (representative data are shown for complexes **2**, **3**, and **5** in Figure 2b,c). In the case of **3**, $\chi_M T$ increases from a value of 6.8 cm^3 K mol^{-1} at 300 K to a maximum value of 7.4 cm^3 K mol^{-1} at 70 K (see Figure 2b). Below 50 K, the data undergo a downturn, likely the result of Zeeman and zero-field splitting. The data for trinuclear bromide **5** and iodide **6** complexes are similar (see Figures S15 and S16 in the SI). The data for the hexanuclear, chloride-bridged complex **2** are nearly double that observed for trinuclear **3**. For **2**, $\chi_M T$ exhibits a maximal value of 12.8 cm^3 K mol^{-1} at 300 K but decreases substantially below temperatures of 120 K (see Figure 2b). Variable-temperature magnetization data were collected for complexes **2**−**6** in the temperature range of 1.8−10 K at fields of 1−7 T. A representative plot of reduced magnetization for **5** is shown in Figure 2c, which features a series of nonsuperimposable

dx.doi.org/10.1021/ic301241s | *Inorg. Chem.* 2012, 51, 10274−10278

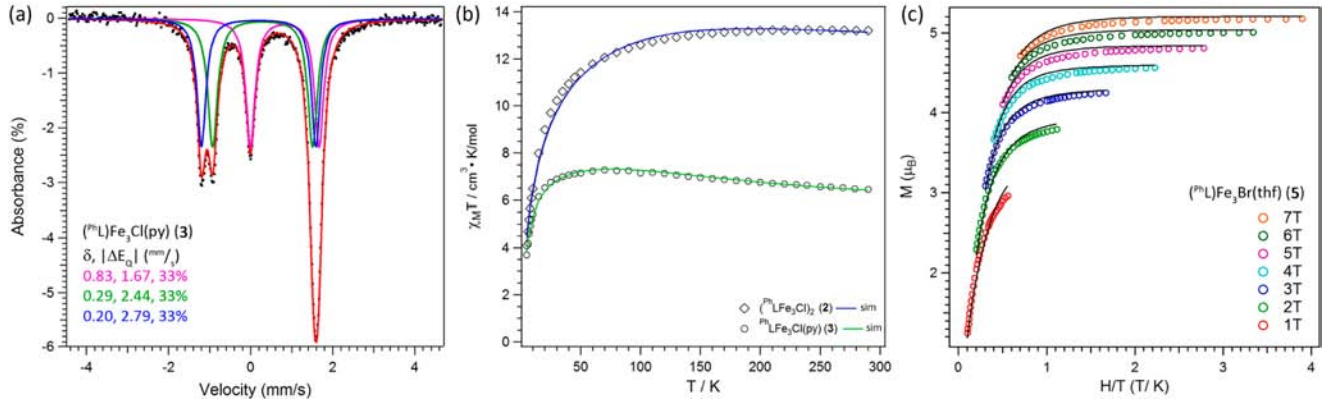

Figure 2. (a) Zero-field ^{57}Fe Mössbauer spectrum obtained at 90 K and spectral fits [δ, $|\Delta E_Q|$ (mm s^{-1})] for **3** [component 1 (magenta), 0.83, 1.67, 33%; component 2 (green), 0.29, 2.44, 33%; component 3 (blue), 0.20, 2.79, 33%]. (b) Variable-temperature magnetic susceptibility data for **2** (diamonds) and **3** (circles) collected in an applied dc field of 0.1 T. The solid lines represent fits to the data as described in the text. (c) Plot of the reduced magnetization for **5** between 1.8 and 10 K at applied fields of 1−7 T.

isofield curves, with the 7 T curve reaching a maximum value of M = 5.4 μ_B at 1.8 K.

On the basis of the Mössbauer spectra, which suggest that each of the oxidized trinuclear cores consists of an isolated ferrous site and a mixed-valent dinuclear unit, we modeled the data using the two-spin Hamiltonian shown in eq 1, where S_1 = 2 for the ferrous site and S_2 represents the mixed-valent diiron unit spin.

$$\hat{H} = -2J(S_1S_2) + \sum D_iS_i^2 + g\mu_B\mathbf{S}\cdot\mathbf{B} \quad (1)$$

The spin state of the diiron $[Fe_2]^{5+}$ unit S_2 will fall in the range of $^1/_2$ for a maximally low-spin state to $^9/_2$ for a maximally high-spin state.[7] The value of S_2 affects data simulations by setting the value for g as well as modulating the effect that D_2 has on the shape of the susceptibility and reduced magnetization curves. Suitable models of the data (where $g \approx 2$) were only obtained when $S_2 = {}^3/_2$ was used in eq 1, suggesting a total spin state of $S = {}^7/_2$ for the trinuclear complex, which is consistent with the room temperature magnetic moments obtained for **3** ($\mu_{spin\text{-}only}$ = 7.94 μ_B for $S = {}^7/_2$). The corresponding simulation using the program *MAGPACK*[8] that best reproduces the susceptibility and reduced magnetization data affords parameters of J = +16 cm^{-1}, D_1 = 36 cm^{-1}, D_2 = −47 cm^{-1}, and g = 2.09. The surprising decrease in D_1 as a function of the halide substitution between **3** (36 cm^{-1}), **5** (14 cm^{-1}), and **6** (14 cm^{-1}) directly opposes the anticipated trend because of the larger spin−orbit coupling in the heavier halides.[9] However, the coordination environment of the halide-bearing ferrous site is altered between the complexes as a result of the halide substitution. Thus, any enhanced magnetic anisotropy imparted by the addition of the heavier halide may be offset by a change in the intrairon spacing (see Table S2 in the SI). The large D_2 values for the $[Fe_2]^{5+}$ unit in **3** (−47 cm^{-1}), **5** (−96 cm^{-1}), and **6** (−110 cm^{-1}) suggest significant separation between the m_S = $\pm{}^3/_2$ and $\pm{}^1/_2$ levels. Though these values are large, they are in accordance with other dinuclear species featuring a large degree of metal−metal orbital overlap, most notably the $[Ru_2]^{5+}$ and $[Ru_2]^{6+}$ complexes, where D values up to 70 and 260 cm^{-1}, respectively, have been observed.[10]

Modifying the Hamiltonian spin expression to account for an additional exchange interaction J_2 (between the two trinuclear subunits mediated through the bridging halides in **2**), we modeled the data for **2** using eq 2).

$$\hat{H} = -2J_1(S_{1_a}S_{2_a} + S_{1_b}S_{2_b}) - 2J_2(S_{1_a}S_{1_b}) + \sum D_iS_i^2 + g\mu_B\mathbf{S}\cdot\mathbf{B} \quad (2)$$

The simulation that best reproduces the data for **2** affords parameters of J_1 = +13 cm^{-1}, J_2 = −1.2 cm^{-1}, D_1 = 40 cm^{-1}, D_2 = −133 cm^{-1}, and g = 2.19. The weak antiferromagnetic coupling between the trinuclear subunits leads to the S = 0 ground state for the hexanuclear, halide-bridged complexes **2** and **4** (see Figures S12 and S14 in the SI), contributing to the downturn in the susceptibility data at lower temperatures. At higher temperatures, the susceptibility data are nearly twice the values observed for trinuclear **3**, consistent with two spin-independent trinuclear subunits in **2**. This assessment is corroborated by the reduced magnetization data for **2** and **4** (see Figures S12 and S14 in the SI).

The electronic structure within the trinuclear cores deviates from that of our previous work, wherein redox was symmetrically distributed within the polynuclear core.[3a,c] In previous examples, bonding metrics within the polynuclear core are affected by direct orbital−orbital interactions between adjacent metal sites. Upon oxidation of the low-spin congener $(^HL)Fe_3(PMe_3)_3$, the contraction observed within the trinuclear core is attributed to the depopulation of a nominally antibonding interaction.[3a] In the present case, chemical oxidation of **1** leads to increased metal−metal interaction within the dinuclear site of oxidation, while simultaneously attenuating the interaction with the lone ferrous site. The iron−anilido [Fe−N 2.078(3) Å] and iron−halide bond metrics for Fe1 in **3** are consistent with a high-spin ferrous assignment. The close iron−iron separation in the oxidized diiron unit $[Fe_2]^{5+}$ suggests significant M−M orbital overlap. The diiron unit is approximated as two edge-sharing square-planar atoms, giving rise to direct orbital interactions, as illustrated in Scheme 2. Population of the 11 valence electrons into this manifold will not fill the three highest-lying σ^* orbitals, which represent $(Fe{-}N)_\sigma{}^*$ and $(Fe{-}Fe)_\sigma{}^*$ interactions, with the latter arising from the antibonding combination of Fe d_{z^2}. Consistent with this model, the average Fe−N distance in **3** [1.936(5) Å] are considerably shorter than high-spin **1** [2.176(5) Å] where these orbital interactions are populated. As illustrated in Scheme 2, this electronic configuration gives rise to the observed $S = {}^3/_2$ for the $[Fe_2]^{5+}$ unit, consistent with our interpretation of the magnetic data.

dx.doi.org/10.1021/ic301241s | *Inorg. Chem.* 2012, 51, 10274−10278

Scheme 2

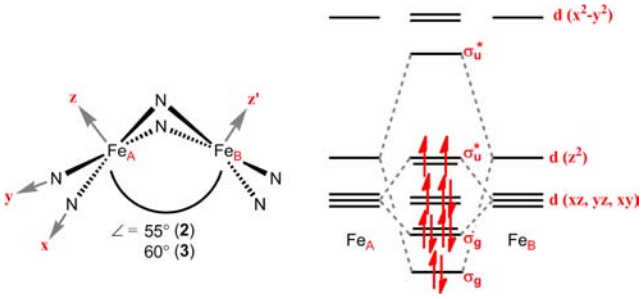

IV. CONCLUSIONS

The above analysis, based on crystallographic, magnetic, and Mössbauer spectral data, suggests a new mechanism by which redox is mediated within polynuclear complexes. In the low-spin regime, oxidation is delocalized throughout the trinuclear core. Mössbauer data obtained upon atom transfer to the high-spin (^{tbs}L)Fe_3(THF) complex suggest that the two-electron oxidation incurred upon nitride formation is core-delocalized.[3b] However, the foregoing data describing the chemical oxidation of high-spin **1** demonstrate that oxidation leads to a trapped valency within a diiron unit, separate from the apparent site of halide capture, with concomitant rearrangement of the trinucleating ligand. These observations are analogous to the previously reported redox-induced electron-transfer reactivity exhibited by redox-active ligands.[11] Typically, such ligand reorganization presents a large energy barrier, but the maximally high-spin formulation of the all-ferrous precursor creates an inherently labile system. Furthermore, the elucidation of this unusual mode of cooperative redox reactivity demonstrates the potential of polynuclear complexes to provide insight into how redox processes may occur within polynuclear metallocofactors in nature.

■ ASSOCIATED CONTENT

Ⓢ Supporting Information

Experimental procedures and spectral data for **2**−**6**, selected crystallographic data and bond lengths for **2**−**6**, and a CIF file for **2**−**6**. This material is available free of charge via the Internet at http://pubs.acs.org.

■ AUTHOR INFORMATION

Corresponding Author

*E-mail: betley@chemistry.harvard.edu.

Notes

The authors declare no competing financial interest.

■ ACKNOWLEDGMENTS

The authors thank Harvard University and the NIH (Grant GM 098395) for financial support, Prof. R. H. Holm for the generous use of his Mössbauer spectrometer, and the Harvard University Center for the Environment for funding (to E.V.E.).

■ REFERENCES

(1) Nitrogenase: (a) Burgess, B. K.; Lowe, D. J. *Chem. Rev.* **1996**, *96*, 2983. (b) Dos Santos, P. C; Igarashi, R. Y.; Lee, H.-I.; Hoffman, B. M.; Seefeldt, L. C.; Dean, D. R. *Acc. Chem. Res.* **2005**, *38*, 208. (c) Hoffman, B. M.; Dean, D. R.; Seefeldt, L. C. *Acc. Chem. Res.* **2009**, *42*, 609. Photosystem II: (d) Nugent, J. *Biochim. Biophys. Acta* **2001**, *1503*, 1. (e) Ferreira, K. N.; Iverson, T. M.; Maghlaoui, K.; Barber, J.; Iwata, S. *Science* **2004**, *303*, 1831. (f) Iwata, S.; Barber, J. *Curr. Opin. Struct. Biol.* **2004**, *14*, 447. N_2O reductase: (g) Brown, K.; Djinovic-Carugo, K.; Haltia, T.; Cabrito, I.; Saraste, M.; Moura, J. J. G.; Moura, I.; Tegoni, M.; Cambillau, C. *J. Biol. Chem.* **2000**, *275*, 41133. (h) Brown, K.; Tegoni, M.; Prudêncio, M.; Pereira, A. S.; Besson, S.; Moura, J. J.; Moura, I.; Cambillau, C. *Nat. Struct. Biol.* **2000**, *7*, 191. (i) Chen, P.; George, S. D.; Cabrito, I.; Antholine, W. E.; Moura, J. G.; Moura, I.; Hedman, B.; Hodgson, K. O.; Solomon, E. I. *J. Am. Chem. Soc.* **2002**, *124*, 744.

(2) (a) Fontecilla-Camps, J. C. *J. Biol. Inorg. Chem.* **1996**, *96*, 3031. (b) Siegbahn, P. E. M. *Inorg. Chem.* **2000**, *39*, 2923. (c) Huniar, U.; Ahlrichs, R.; Coucouvanis, D. *J. Am. Chem. Soc.* **2004**, *126*, 2588.

(3) (a) Zhao, Q.; Betley, T. A. *Angew. Chem., Int. Ed.* **2011**, *50*, 709. (b) Powers, T. M.; Fout, A. R.; Zheng, S.-L.; Betley, T. A. *J. Am. Chem. Soc.* **2011**, *133*, 3336. (c) Zhao, Q.; Harris, T. D.; Betley, T. A. *J. Am. Chem. Soc.* **2011**, *133*, 8293. (d) Harris, T. D.; Zhao, Q.; Hernández Sánchez, R.; Betley, T. A. *Chem. Commun.* **2011**, *47*, 6344. (e) Harris, T. D.; Betley, T. A. *J. Am. Chem. Soc.* **2011**, *133*, 13852. (f) Fout, A. R.; Zhao, Q.; Xiao, D. J.; Betley, T. A. *J. Am. Chem. Soc.* **2011**, *133*, 16750. (g) Eames, E. V.; Harris, T. D.; Betley, T. A. *Chem. Sci.* **2012**, *3*, 407.

(4) (a) Adams, R. D. *J. Organomet. Chem.* **2000**, *600*, 1. (b) Suzuki, H. *Eur. J. Inorg. Chem.* **2002**, 1009. (c) Dyson, P. J. *Coord. Chem. Rev.* **2004**, *248*, 2443. (d) Pap, J. S.; DeBeer George, S.; Berry, J. F. *Angew. Chem., Int. Ed.* **2008**, *47*, 10102.

(5) Gomberg, M. *J. Am. Chem. Soc.* **1900**, *22*, 757.

(6) (a) Balch, A. L.; Holm, R. H. *J. Am. Chem. Soc.* **1966**, *88*, 5201. (b) Warren, L. F. *Inorg. Chem.* **1977**, *16*, 2814. (c) Chaudhuri, P.; Verani, C. N.; Bill, E.; Bothe, E.; Weyhermüller, T.; Wieghardt, K. *J. Am. Chem. Soc.* **2001**, *123*, 2213. (d) Anillo, A.; Diaz, M. R.; Garcia-Granda, S.; Obeso-Rosete, R.; Galindo, A.; Ienco, A.; Mealli, C. *Organometallics* **2004**, *23*, 471. (e) Bill, E.; Bothe, E.; Chaudhuri, P.; Chlopek, K.; Herebian, K.; Kokatam, S.; Ray, K.; Weyhermüller, T.; Neese, F.; Wieghardt, K. *Chem.—Eur. J.* **2005**, *11*, 204. (f) Chlopek, K.; Bill, E.; Weyhermüller, T.; Wieghardt, K. *Inorg. Chem.* **2005**, *44*, 7087.

(7) (a) Drüeke, S.; Chaudhuri, P.; Pohl, K.; Wieghardt, K.; Ding, X.-Q.; Bill, E.; Sawaryn, A.; Trautwein, A. X.; Winkler, H.; Gurman, S. J. *Chem. Commun.* **1989**, 59. (b) Ding, X.-Q.; Bominaar, E. L.; Bill, E.; Winkler, H.; Trautwein, A. X.; Drüeke, S.; Chaudhuri, P.; Wieghardt, K. *J. Chem. Phys.* **1990**, *92*, 178. (c) Dutta, S. K.; Ensling, J.; Werner, R.; Flörke, U.; Haase, W.; Gütlich, P.; Nag, K. *Angew. Chem., Int. Ed.* **1997**, *36*, 152. (d) LeCloux, D. D.; Davydov, R.; Lippard, S. J. *J. Am. Chem. Soc.* **1998**, *120*, 6810. (e) Lee, D.; Krebs, C.; Huynh, B. H.; Hendrich, M.; Lippard, S. J. *J. Am. Chem. Soc.* **2000**, *122*, 5000. (f) Hazra, S.; Sasmal, S.; Fleck, M.; Grandjean, F.; Sougrati, M. T.; Ghosh, M.; Harris, T. D.; Bonville, P.; Long, G. J.; Mohanta, S. *J. Chem. Phys.* **2011**, *134*, 174507.

(8) Borrás-Almenar, J. J.; Clemente-Juan, J. M.; Coronado, E.; Tsukerblat, B. S. *J. Comput. Chem.* **2001**, *22*, 985.

(9) Karunadasa, H. I.; Arquero, K. D.; Berben, L. A.; Long, J. R. *Inorg. Chem.* **2010**, *49*, 4738.

(10) (a) Bennett, M. J.; Caulton, K. G.; Cotton, F. A. *Inorg. Chem.* **1969**, *8*, 1. (b) Angaridis, P.; Cotton, F. A.; Murillo, C. A.; Villagran, D.; Wang, X. *J. Am. Chem. Soc.* **2005**, *127*, 5008. (c) Barral, M. C.; Gallo, T.; Herrero, S.; Jimenez-Aparicio, R.; Torres, M. R.; Urbanos, F. A. *Inorg. Chem.* **2006**, *45*, 3639. (d) Barral, M. C.; Gallo, T.; Herrero, S.; Jimenez-Aparicio, R.; Torres, M. R.; Urbanos, F. A. *Chem.—Eur. J.* **2007**, *13*, 10088. (e) Chiarella, G. M.; Cotton, F. A.; Murillo, C. A.; Young, M. D.; Zhao, Q. *Inorg. Chem.* **2010**, *49*, 3051.

(11) (a) Min, K. S.; DiPasquale, A. G.; Golen, J. A.; Rheingold, A. L.; Miller, J. S. *J. Am. Chem. Soc.* **2007**, *129*, 2360. (b) Min, K. S.; DiPasquale, A. G.; Rheingold, A. L.; White, H. S.; Miller, J. S. *J. Am. Chem. Soc.* **2009**, *131*, 6229.